

1998

# Measurement of thin liquid film drainage using a novel high-speed impedance analyzer

Kevin O. Hool

Robert C. Saunders

Harry J. Ploehn

University of South Carolina - Columbia, ploehn@cec.sc.edu

Follow this and additional works at: [https://scholarcommons.sc.edu/eche\\_facpub](https://scholarcommons.sc.edu/eche_facpub)

 Part of the [Chemical Engineering Commons](#)

---

## Publication Info

*Review of Scientific Instruments*, 1998, pages 3232-3239. Copyright 1998 American Institute of Physics. This article may be downloaded for personal use only. Any other use requires prior permission of the author and the American Institute of Physics. This article appeared in *Review of Scientific Instruments* and may be found at <http://link.aip.org/link/doi/10.1063/1.1149088>.

DOI:10.1063/1.1149088

This Article is brought to you by the Chemical Engineering, Department of at Scholar Commons. It has been accepted for inclusion in Faculty Publications by an authorized administrator of Scholar Commons. For more information, please contact [dillarda@mailbox.sc.edu](mailto:dillarda@mailbox.sc.edu).

## Measurement of thin liquid film drainage using a novel high-speed impedance analyzer

Kevin O. Hool, Robert C. Saunders, and Harry J. Ploehn

Citation: *Rev. Sci. Instrum.* **69**, 3232 (1998); doi: 10.1063/1.1149088

View online: <http://dx.doi.org/10.1063/1.1149088>

View Table of Contents: <http://rsi.aip.org/resource/1/RSINAK/v69/i9>

Published by the [American Institute of Physics](#).

---

### Related Articles

Effect of plumes on measuring the large scale circulation in turbulent Rayleigh-Bénard convection  
[Phys. Fluids 23, 095110 \(2011\)](#)

Note: Anti-strong-disturbance signal processing method of vortex flowmeter with two sensors  
[Rev. Sci. Instrum. 82, 096105 \(2011\)](#)

Droplet collisions and interaction with the turbulent flow within a two-phase wind tunnel  
[Phys. Fluids 23, 085105 \(2011\)](#)

The influence of pressure relaxation on the structure of an axial vortex  
[Phys. Fluids 23, 073101 \(2011\)](#)

Artificial lateral line canal for hydrodynamic detection  
[Appl. Phys. Lett. 99, 023701 \(2011\)](#)

---

### Additional information on Rev. Sci. Instrum.

Journal Homepage: <http://rsi.aip.org>

Journal Information: [http://rsi.aip.org/about/about\\_the\\_journal](http://rsi.aip.org/about/about_the_journal)

Top downloads: [http://rsi.aip.org/features/most\\_downloaded](http://rsi.aip.org/features/most_downloaded)

Information for Authors: <http://rsi.aip.org/authors>

### ADVERTISEMENT



**AIP**Advances

*Submit Now*

**Explore AIP's new  
open-access journal**

- **Article-level metrics  
now available**
- **Join the conversation!  
Rate & comment on articles**

# Measurement of thin liquid film drainage using a novel high-speed impedance analyzer

Kevin O. Hool

*CR&D Engineering Research and Process Development Laboratory, The Dow Chemical Company, Midland, Michigan 48641*

Robert C. Saunders

*Intertec Design, Inc., Midland, Michigan 48640*

Harry J. Ploehn<sup>a)</sup>

*Department of Chemical Engineering, University of South Carolina, Swearingen Engineering Center, Columbia, South Carolina 29208*

(Received 4 February 1998; accepted for publication 14 June 1998)

This work describes the design and implementation of a new instrument, called the thin film impedance analyzer, which measures the rate of drainage of thin oil films. The instrument forms an oil film by elevating a planar oil–water interface into a water drop hanging from a stainless steel capillary tube immersed in the oil. The instrument measures the magnitude of the impedance of the matter between the capillary tube and a screen electrode immersed in the lower water phase. Under appropriate conditions, the capacitance of the oil film dominates the impedance. The instrument records the increase in the magnitude of the admittance associated with the draining and thinning of the oil film. The features of the drainage curves vary considerably with the type, amount, and location of surfactants in the oil and water phases, as well as with user-specified values of drop volume, drop equilibration time, and extent of drop compression. For this reason, the instrument has utility as a screening tool for selecting surfactants for emulsion formulations. Potential future uses include accelerated prediction of emulsion stability and extraction of oil–water interfacial rheological parameters. © 1998 American Institute of Physics. [S0034-6748(98)01609-8]

## I. INTRODUCTION

The rate of coalescence of liquid droplets in emulsions has long been known to depend primarily upon the properties of the phase interface between the dispersed and continuous phases. Interfacial properties, and thus the stability of emulsions and foams, are controlled through the use of surface-active agents (surfactants) that accumulate at interfaces between phases of differing polarity. Indeed, the ability to tailor interfacial properties through appropriate selection and utilization of surfactants serves as the foundation for many lucrative businesses, including emulsion polymerization, personal care and household cleaning products, and processed foods.

Surfactants, including small molecule amphiphiles, copolymers, and solid colloidal particles, perform two basic functions in emulsions: they control droplet size, and they alter the droplet coalescence rate. Surfactants adsorb at oil–water interfaces and thereby reduce the interfacial tension. In addition, surfactant adsorption alters interfacial rheological properties through various mechanisms.

To make efficient use of the work supplied to produce the droplets, the interfacial film of surfactant should also promote emulsion stability by slowing that rate of coalescence of the droplets. Coalescence of two drops requires drainage and thinning of the intervening liquid film of the

continuous phase, followed by rupture of the thinned film. Considerable effort has been devoted to developing an understanding of the basic mechanisms governing the drainage and rupture of thin liquid films. Numerous reviews are available.<sup>1–3</sup> Invariably, interfacial surfactant plays a central role in all proposed drainage and rupture mechanisms. Proper selection and efficient use of surfactants for different end-use applications motivates the need for experimental techniques for characterizing and quantifying the effect of surfactants on thin film drainage and rupture.

Over the years, considerable research has focused on the drainage and rupture of foam films (i.e., liquid films bounded by gas phases). Interferometric techniques have provided a convenient means for quantifying the time and spatial dependence of film thickness. Reviews<sup>4</sup> and recent literature<sup>5–8</sup> provide more details on this method. We are not aware of any successful use of interferometry to quantify the rate of drainage of emulsion films (i.e., liquid films bounded by other liquid phases). Velikov *et al.*<sup>8</sup> reported results for the tendency of emulsion films to rupture. However, they did not report drainage rates because the emulsion films ruptured at thicknesses greater than those probed by interferometry.

In fact, instruments devoted to measurement of the rate of drainage of emulsion films (i.e., liquid films bounded by other liquid phases) are not widely available. Instead, attention has focused on quantifying film rupture or droplet coalescence rates. One empirical approach for predicting emulsion stability has been single droplet coalescence

<sup>a)</sup> Author to whom correspondence should be addressed.

experiments.<sup>1</sup> For example, Hodgson and Lee<sup>9</sup> described an apparatus and manual technique for forming a single drop, pressing it into a planar liquid–liquid interface, measuring the time to coalescence. Scheele and Ung<sup>10</sup> used high-speed photography to visualize droplet collisions and presented a model to rationalize observed coalescence behavior. Flumerfelt and co-workers<sup>11</sup> used a modified spinning drop apparatus to perform droplet–droplet coalescence experiments, leading to estimates of dilatational viscosity for films with very low interfacial tensions.

The underlying premise of these experiments is that the coalescence time for a single drop pressed into a liquid–liquid interface (or for an isolated pair of drops) provides an estimate for the stability of an emulsion containing many droplets. However, the methods described in the literature do not provide information on the thickness of the draining film as a function of time, nor do they give a direct measure of any interfacial properties. Instead, coalescence time data are interpreted through simple models of thin film drainage to calculate rheological figures of merit, such as “apparent” interfacial viscosity. Such metrics may rationalize coalescence data, discriminate between effective and ineffective surfactant formulations, and provide useful predictions of emulsion stability. Unfortunately, published techniques require intensive manual labor to set up and operate and do not use any form of microprocessor control. We are not aware of any commercial instrumentation that would enable researchers to efficiently build a database of knowledge required for rational selection of surfactants for emulsion applications.

This article describes a new instrument<sup>12</sup> for measuring the rate of drainage of a thin liquid film formed by pressing a drop into a planar liquid–liquid interface. The instrument measures impedance to quantify the drainage rate. Consequently, we refer to the instrument as the thin film impedance analyzer (TFIA). After outlining the basic measurement principles and design of the TFIA, we provide illustrative experimental results that demonstrate the utility of the approach.

## II. INSTRUMENT DESIGN

### A. Measurement principle

The TFIA grows a pendant water drop of known volume at the end of a stainless steel capillary tube suspended in a bulk oil phase (Fig. 1). The oil phase floats on top of a bulk water phase, forming a planar oil–water interface. A mechanical stage elevates the bulk oil and water phases so that the drop presses into the oil–water interface, thus trapping a thin film of oil between the water drop and the lower water phase. Buoyant and interfacial forces exerted on the film cause the oil to flow laterally out of the film, leading to thinning of the film. Because the radii of curvature of the interfaces are much greater than the thickness of the film, the drainage approximates that of a liquid film compressed between parallel planes.

A stainless steel screen electrode is immersed in the lower water phase. The TFIA applies a sinusoidal voltage with known frequency and amplitude between the steel capillary and screen electrodes and measures the amplitude of

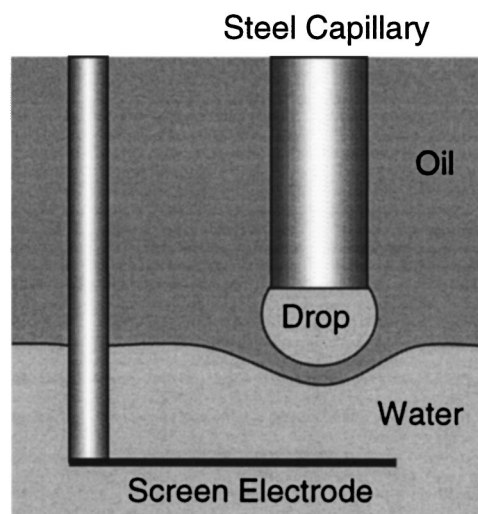


FIG. 1. Configuration of liquid phases and electrodes in the TFIA coalescence cell.

the alternating current. The measured current amplitude is inversely proportional to the magnitude of the impedance (or directly proportional to the magnitude of the admittance) of the material between the electrodes. Although the equivalent circuit of the material may not be simple, the circuit element associated with the thin oil film can be represented as a plane parallel capacitor. As the trapped oil film drains, the capacitance of the film and the impedance magnitude both increase. The experiment ends when the film ruptures and the water drop coalesces with the lower water phase.

By recording the time dependence of the magnitude of the admittance, the TFIA measures the rate of drainage of the thin oil film. The measured signal (“count”), proportional to the admittance magnitude, depends on a variety of controlled instrumental parameters as well as the type, concentration, and location of surfactants in the liquids. With the development of an appropriate equivalent circuit model, the true film thickness could be regressed from the measured count. A hydrodynamic model of thin film drainage could then be used to estimate interfacial rheological properties from thickness versus time data. The development of these models will be the subject of a future report.

### B. Apparatus

The TFIA<sup>12</sup> consists of six principal components: a coalescence cell, a precision syringe pump, a Z-World<sup>®</sup> Little Giant<sup>®</sup> microcontroller board, a custom-designed analog signal processing board, a stepper motor-driven stage with microcontroller, and a user terminal with disk data storage. Figure 2 shows a block diagram illustrating the interconnections among these components.

#### 1. Coalescence cell and syringe pump

The coalescence cell assembly consists of a 50 mL borosilicate glass beaker containing the bulk oil and water phases, a mount that holds the beaker, the steel capillary tube, and a cell housing for electromagnetic shielding. The capillary tube requires a special design to successfully form a stable pendant drop when the interfacial tension is low. In

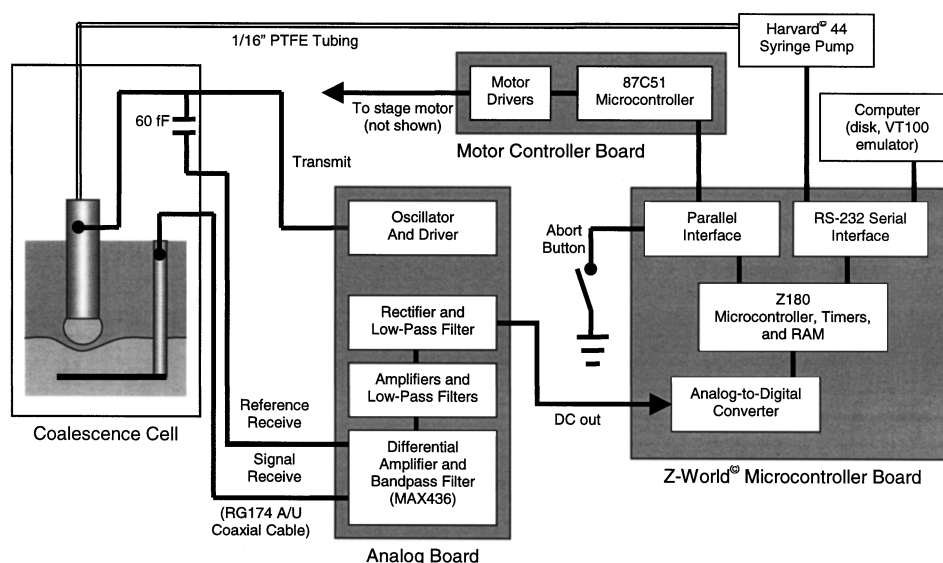


FIG. 2. Block diagram of major TFIA components.

the design of an instrument for measurement of dynamic interfacial tension,<sup>13</sup> a special capillary was designed to minimize the contact area between the capillary and the drop, enabling accurate and reproducible estimates of the force required for drop detachment. However, this design was not suitable for hanging large pendant drops, especially for low values of the oil–water interfacial tension.

The TFIA capillary employs 1/32 in. o.d. stainless steel tubing with an orifice machined to present an inverted cone with a 45° cone angle.<sup>12</sup> This design provides a large surface area for secure attachment of large pendant drops with low interfacial tension (as low as 0.5 dyn/cm). During an experiment, when elevation of the oil–water interface compresses the drop, the applied force is evenly distributed around the perimeter, thus minimizing the tendency for the drop to be pushed off of the capillary axis. Extensive experimentation has shown that this design leads to superior reproducibility in film drainage data.

Teflon tubing (1/16 in. o.d.) connects the capillary to a precision syringe pump (Harvard® model 44). The pump pushes an aqueous fluid through the tubing to form the pendant drop. Typical drop volumes are between 0.5 and 20  $\mu\text{L}$ .

The cell housing minimizes radio frequency electromagnetic interference that could reduce the accuracy of the measurements. The housing consists of a cylindrical steel can with a removable cap and bottom. The housing bottom is attached to a base plate that also holds the stepper motor for the stage. The diameter (105 mm) and height (145 mm) of the housing provide a comfortable fit over the coalescence cell. The stage mount that holds the beaker passes through the housing to the stepper motor via a cutout near the bottom. Two rectangular openings on either side of the housing provide convenient access to the sample and enable viewing of coalescence events.

A steel sheet divides the interior of the housing into upper and lower portions and serves as the mounting plate for the capillary and the stem holding the screen electrode. Flexible stainless steel screens divide the upper portion of

the housing into three sections in order to shield the transmit line, the receive line, and the reference capacitor from one another, thus minimizing internal electrical interference (crosstalk). The shielded terminal of a SMB coaxial connector is silver soldered to the side of the steel capillary. A coaxial stainless steel tube shields the capillary and contacts to the shielding of the SMB connector. A coaxial steel tube also isolates the stem holding the screen electrode. Coaxial cable (type RG-174A/U, 50  $\Omega$ ) connects both electrodes to SMA coaxial connectors mounted in the housing wall. All of these precautions reduce the stray capacitance within the cell.

## 2. Motorized stage

The TFIA forms a thin oil film by elevating the oil–water interface in the beaker into contact with the pendant water drop. The beaker rests on a stepper motor-driven mechanical stage that performs this function. The capillary and screen electrode stem, mounted on the housing, remain motionless. The stepper motor, a Klinger® MF04CC linear positioner, is mounted on the TFIA base that also holds the cell housing bottom plate. The mounting enables vertical travel of the positioner. The stage holding the beaker is attached to the positioner slide.

A DC servomotor drives the motion of the stage. The motor has an integral magnetic quadrature encoder that feeds position data back to the control electronics. The encoder has a resolution of 0.06  $\mu\text{m}$ , allowing accurate determination of position. However, the positioner cannot be moved to a given position with this accuracy due to the momentum of the servomotor and stage. The motor requires 12 V and draws 90 mA at its full operating speed of 300  $\mu\text{m/s}$ . The positioner has a total range of 8 mm with normally closed limit microswitches at the ends of travel. The control electronics will be described in the next section.

### 3. Electronic components

The TFIA quantifies the magnitude of the impedance of the coalescence cell and its contents via a differential measurement between the cell and a reference capacitor (60 fF) mounted inside the coalescence cell housing. An oscillator/driver circuit on the custom-built analog board (Fig. 2) generates a sinusoidal voltage at a frequency of 4 MHz with an amplitude of 1.0 V. The transmit line carries this signal to the coalescence cell and reference capacitor. The signals from the screen electrode and reference capacitor pass through the receive and reference lines, respectively, to a differential amplifier and bandpass filter (MAX436) on the analog board. The signal undergoes further filtering, rectification, and amplification before passing to the 12 bit analog-to-digital converter on the Z World® Little Giant® microcontroller board.

The Little Giant® microcontroller provides automated control of all of the instrument's functions. The Little Giant® sends instructions to the Harvard® syringe pump and data to the user terminal via the RS-232 serial interface. The control program, written in the C language, resides in the EPROM of the Little Giant®.

The calculation time required for both real-time data sampling and accurate positioning of the stage dictate the use of a separate controller for the positioner motor. A separate motor controller also enables simultaneous data sampling and motor control. The positioner motor is controlled by an Intel® 87C51FB microcontroller, mounted on a custom circuit board with power metal-oxide-semiconductor field-effect transistor (MOSFETs) for motor control. The on-chip EPROM of the Intel® 87C51FB was programmed using a cross-assembler package. A parallel interface connects the motor microcontroller to the Little Giant® microcontroller.

The need for accurate positioning of the stage necessitated the development of an active braking system for the stage motor. The traditional method of stopping a motor quickly is to short circuit the motor armature, transforming the motor into a generator forced to drive a low resistance, large current load. Early versions of the TFIA accomplished this via a small relay mounted on the circuit board. Unfortunately, the surge currents from even a small motor proved to be too large for a small relay to handle. A relay with the necessary current and voltage specifications would be unacceptably large. This technique also has the disadvantage that the loading force opposing the motor diminishes with motor speed, thus permitting an unacceptable amount of coast regardless of the initial speed of the motor.

At present, the TFIA stops the positioner motor by reversing the power and driving the motor in the opposite direction until the magnetic encoder indicates that the motor has stopped. The power is then turned off before the motor develops any reverse momentum. The current and voltage requirements of this technique are easily handled by the MOSFETs (14 A, 60 V) present on the motor microcontroller board. The Intel® 87C51FB controller was fast enough to switch the reverse power off at the right moment to prevent significant reverse movement of the motor. This technique permits stage positioning to within a few microns of a speci-

fied position and allows fast braking using no additional electronic components.

### 4. Operating environment

Interfacial measurements are quite sensitive to thermal variations and vibrations. Temperature variations in the syringe and Teflon tubing can produce significant volume changes in the fluid and thus the pendant drop. The drop volume controls the contact area between the drop and the oil-water interface as well as the initial film thickness of the oil film. The measured signal is sensitive to variations in these quantities. To avoid long-term drift of the measured signal, a Plexiglas box encloses the coalescence cell and housing, the positioner, and the syringe pump. Communication cables pass through a small hole. The enclosure is mounted on vibration-dampening pads to minimize this source of experimental noise.

We observed low frequency noise in the signal on partly cloudy days, but not on overcast or clear days. Apparently, even a north-facing window admits sufficient thermal radiation to alter the temperature of the syringe contents. A cardboard shade now shields the TFIA from thermal radiation from windows and other sources. This experience highlights the need for proper environmental controls when making measurements sensitive to small fluid volume variations.

## III. MEASUREMENT MODES

The software for the TFIA provides a variety of experimental modes that can be easily modified and allow considerable flexibility in the user's choice of experimental parameters. A simple command language has been developed to represent all functions of the instrument. Experiments are programmed as short lists of four-letter mnemonics with single numeric parameters. The mnemonics are tokenized and interpreted by the C language routine responsible for executing the respective instrument functions. Three experimental modes have been developed to date.

### A. Static drop mode

This experimental mode examines the thinning of oil films subjected to a force applied by the static compression of a drop of fixed volume. Figure 3 depicts the sequence of events. First, the stage raises the planar oil-water interface to immerse the tip of the capillary; and then lowers the interface to its initial position [Fig. 3(a)]. At the same time, the instrument monitors the signal (called the count, proportional to the admittance magnitude) from the coalescence cell. The wetting operation serves two purposes: it wets the capillary to ensure a consistent residual amount of liquid on the capillary tip; and it locates the position of the capillary tip by the jump in measured count that occurs upon contact with the interface.

Next, the syringe pump grows a drop with a user-specified volume. The drop remains pendant on the capillary for a user-specified wait period to allow equilibration of the water drop-oil interface [Fig. 3(b)]. After the wait period, the stage raises the planar oil-water interface while simultaneously monitoring the count signal. The TFIA records the

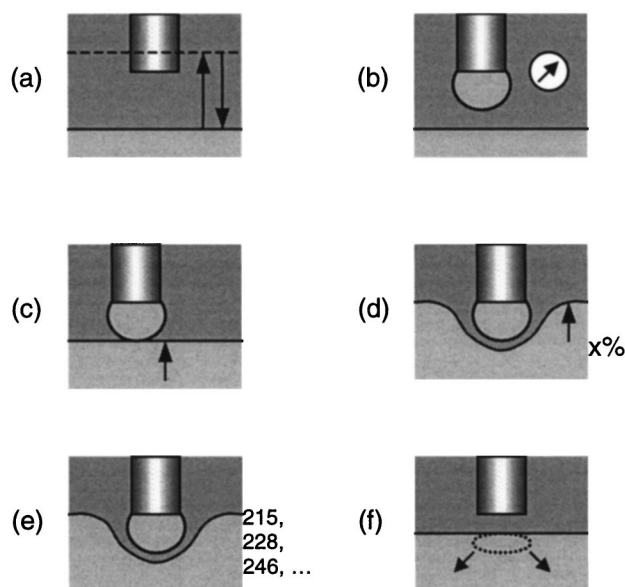


FIG. 3. Sequence of events in a static drop experiment.

position of the bottom surface of the drop [Fig. 3(c)] when the count exceeds a user-specified threshold. The drop height equals the difference between the positions of the capillary tip and the bottom of the drop. The stage continues to raise the oil–water interface, compressing the pendant drop to a user-specified percentage of the drop height [Fig. 3(d)].

At this point, the TFIA begins reporting count values at a user-specified data rate [Fig. 3(e)]. Each count value actually represents the average of 50 discrete sampling events, even at the maximum collection rate of 40 data points per second. Sampling continues until the drop coalesces with the lower water phase [Fig. 3(f)]. A sharp drop in the measured count marks the coalescence event. The entire sequence of events may be repeated automatically for a user-specified number of drops. Figure 4 shows typical results (measured count versus time) for a set of film drainage experiments performed under identical conditions.

### B. Dynamic drop mode

This experimental mode examines the thinning of oil films subjected to a varying force created by a growing water

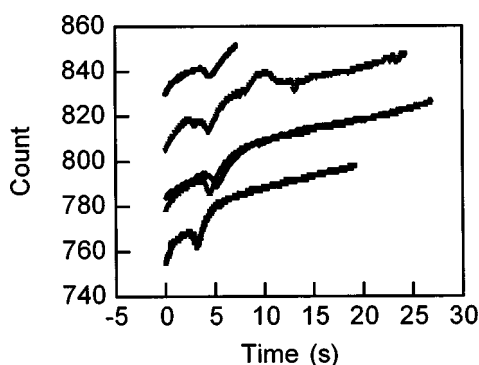


FIG. 4. Typical count vs time data from static drop experiments for multiple drops. The films consist of dodecane; the water phases contain 250 ppm Neodol 91-6 (4  $\mu$ L drops, 20% compression).

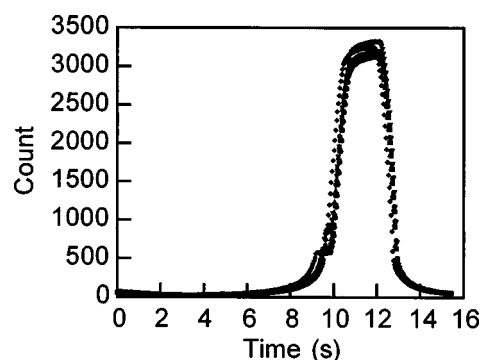


FIG. 5. Typical count vs time data from an approach–recede experiment for multiple compressions of the same drop. The films consist of dodecane; the water phases contain 2500 ppm SDS (4  $\mu$ L drop, 25% compression).

drop. As in the static drop mode, the experiment begins with the wetting of the capillary tip by the oil–water interface. The interface is withdrawn to a user-specified distance from the capillary tip. After a user-defined wait period, the syringe grows a water drop at a user-specified rate. At the same time, the instrument samples and reports the measured count. The experiment proceeds until the drop coalesces with the lower water phase. This cycle may be repeated automatically as many times as specified by the user.

### C. Approach–recede mode

The approach–recede mode traces its origin to the work of Hartland,<sup>14</sup> who employed a rigid aluminum sphere in place of the pendant liquid drop. This mode examines the thinning of oil films while avoiding coalescence of the water drop with the lower water phase. This permits multiple drainage runs using the same drop. For slowly draining films, the approach–recede mode can be used to investigate the effect of varying contact area on the measured count signal.

As in the other modes, the stage first raises the oil–water interface to wet the capillary and locate its tip. The interface is then lowered to its initial position. The syringe pump grows a water drop, followed by a wait period for equilibration. As in the static drop mode, the stage raises the interface and compresses the drop to a user-specified percentage of the drop height. At the same time, the instrument samples and reports count data. Instead of holding the compression at a fixed value, the stage immediately lowers the interface to its initial position while count data continues to be reported. Figure 5 shows typical approach–recede data for multiple drainage runs performed using the same drop.

### D. Other software features

The TFIA software includes extensive error checking for both experiment command list errors as well as erratic events in the coalescence cell itself. Bridging between the capillary and the lower water phase, premature drop detachment, and other mishaps are automatically detected, aborting the experimental run. All of the error routines and the user abort switch on the front panel take the user to the data menu, where the experiments normally finish, so that the user has the option of recovering any data taken up to that point. The program also allows user-specified positioning of the stage

outside of an experimental run. Default values for the three experimental modes are stored in EPROM for recovery on system startup, saving the user the time of repeatedly entering the same parameters for a sequence of runs. The user can change these defaults at any time outside of a run.

#### IV. DATA ANALYSIS

In our film drainage experiments performed to date, the static drop mode has been used most frequently. The count versus time data in Fig. 4 is typical: the drainage curves have similar shapes, but the starting count values differ by about  $\pm 5\%$ . In most cases, plotting the data as count difference versus time superposes the curves reasonably well, demonstrating the reproducibility of the measurements.

We have begun to analyze the data using a rudimentary model that, despite several assumptions, yields interesting insights. The measured count value,  $C$ , is proportional to the magnitude of the admittance of the coalescence cell and its contents. For the purposes of this preliminary analysis, we assume that the admittance is dominated by the capacitance of the oil film,  $C_f$ , so that

$$C = GC_f, \quad (1)$$

where  $G$  is a gain factor. Second, the film capacitance can be treated as that of a plane parallel capacitor with contact area  $A$ , film thickness  $\delta$ , and dielectric permittivity  $\epsilon$ , giving

$$C_f = \frac{\epsilon A}{\delta}. \quad (2)$$

Finally, we require a hydrodynamic model to describe the rate of change of the film thickness. The classic model proposed by Reynolds<sup>15</sup> leads to

$$\frac{d\delta}{dt} = -\frac{8\pi F \delta^3}{3n^2 \mu A^2}, \quad (3)$$

where  $F$  is the applied compression force,  $\mu$  is the oil viscosity, and  $n$  is a parameter associated with the mobility of the oil–water interfaces. For rigid, immobile interfaces, the Reynolds model requires  $n=2$ . The generalization of the Reynolds model for mobile liquid–liquid interfaces treats  $n$  as a parameter with values between 0 and 2. For simplicity, we assume that only the film thickness varies with time. Combining Eqs. (1)–(3) and integrating yields

$$C^2 - C_0^2 = \frac{16\pi \epsilon^2 FG}{3n^2 \mu} t, \quad (4)$$

where  $C_0$  is the measured count value at time  $t=0$ . Equation (4) suggests plotting the difference in the square of the measured count as a function of time. The results reported in the next section are presented in this way.

#### V. RESULTS AND DISCUSSION

##### A. Experimental procedures and materials

Before every experiment, all surfaces exposed to either phase were thoroughly rinsed in deionized water at least three times or until no trace of contamination was visible. The steel capillary was washed in a water/acetone mixture in

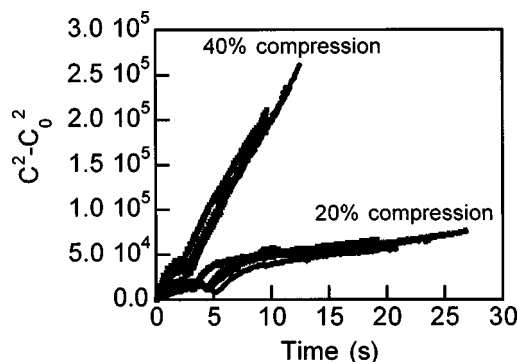


FIG. 6. Effect of percentage compression on the drainage of dodecane films. The water phases contain 250 ppm Neodol 91-6 (4  $\mu$ L drops).

an ultrasonic bath whenever the surfactant type was changed, between each run when a polymeric surfactant had been used, and whenever contamination was suspected. The instrument's electronics were periodically calibrated using a known differential capacitance.

For all experiments, the oil phase was carefully layered over the lower aqueous phase by hand using a glass piston syringe with a stainless steel needle. The planar oil–water interface was allowed to equilibrate for at least five minutes before the beginning of an experiment. The instrument output signal was zeroed with the steel capillary in its working position before a drop was grown. Many experiments involved an appreciable amount of surfactant, producing low interfacial tension values. Consequently, care was taken to prevent unwanted emulsification. Water drops were grown to the desired volume at a rate of 40  $\mu$ L/min and allowed to equilibrate for two minutes.

The experiments described here used deionized water as the aqueous phase and dodecane as the oil phase. Surfactants may be dissolved in either or both phases. A variety of surfactants have been studied, including many from the Tween®, Span®, and Methocel® families. Most of the experiments described here used Neodol® 91-6, a monomeric, nonionic alcohol ethoxylate surfactant. This Neodol's hydrophile–lipophile balance (HLB) value (12.5) makes it soluble in either the water or oil phases. Also, we report some results for sodium dodecyl sulfate (SDS), a common anionic surfactant.

##### B. Film drainage curves

Figure 6 illustrates the effect of varying percentage compression on the drainage rate of dodecane films. Increasing the percentage compression (elevation distance of the oil–water interface relative to the drop bottom divided by the initial drop height) produces a greater buoyant force exerted by the lower water phase on the oil film. The water drops (4  $\mu$ L) and the lower water phase contained 250 ppm Neodol 91-6 surfactant. For both 20% and 40% compressions, the drainage curves for multiple drops superimpose, showing that the drainage curves are reproducible. The films drained more quickly when the compression increased from 20% to 40%. Equations (1) and (2) indicate that larger values of the measured count imply thinner films. Thus the drainage curves in Fig. 6 suggest that, at the same drainage time, greater percentage compression produced thinner films.



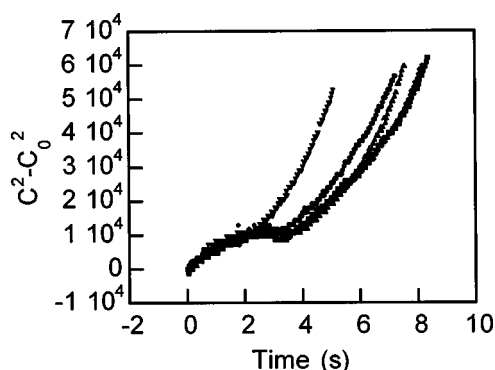


FIG. 7. Drainage of dodecane films under larger water drops. The water phases contain 250 ppm Neodol 91-6 (11  $\mu$ L drops, 20% compression).

These results are consistent with the expectation that increasing the applied (buoyant) force accelerates the film drainage rate.

The drainage curves in Fig. 6, plotted according to Eq. (4), display nonlinear time dependence during the early stages of film drainage. The nonlinearity suggests that the experimental conditions violate one or more of the assumptions that led to Eq. (4). For example, studies of the drainage of aqueous foam films<sup>16</sup> demonstrate that the film's bounding interfaces may not be planar during the first part of the film drainage process. Furthermore, the force, area, and Reynolds parameter ( $n$ ) in Eq. (3) may initially depend on time. At longer times, the drainage curves in Fig. 7 are linear, suggesting that the Reynolds model, Eq. (4), might be suitable for the later stages of oil film drainage. The slopes of the drainage curves increase with percent compression, consistent with an increasing value of  $F$  in Eq. (4). Drainage curves from many other systems, however, do not display linear time dependence when the data are plotted according to Eq. (4).

Drop volume also has a significant effect on the drainage behavior. Drainage curves for dodecane films formed by the compression of 11  $\mu$ L water drops (Fig. 7) may be compared with corresponding data for 4  $\mu$ L drops (Fig. 6). The reproducibility of the drainage curves generally decreases as the drop volume increases, possibly due to larger drop-to-drop volume variations. Larger drops obviously have greater volumes and initial heights than smaller drops. For a specified value of percentage compression, the (buoyant) force applied by raising the oil-water interface increases with the drop volume. Consequently, the film drainage rate increases with drop volume at fixed percentage compression. Finally, we see significant differences in the time dependence of the drainage behavior for varying drop volumes.

Surfactant concentration has an important effect on the drainage behavior. Figure 8 shows that an increase in the Neodol 91-6 concentration in the aqueous phase accelerates the rate of drainage of dodecane films. Although this observation may seem counterintuitive, theoretical models that account for both bulk and interfacial diffusion of surfactant<sup>17</sup> predict this trend. The oil flow out of the film draws surfactant along the oil-water interfaces from the center toward the edges of the film, creating an interfacial tension gradient that opposes the bulk flow and retards drainage. This is known as

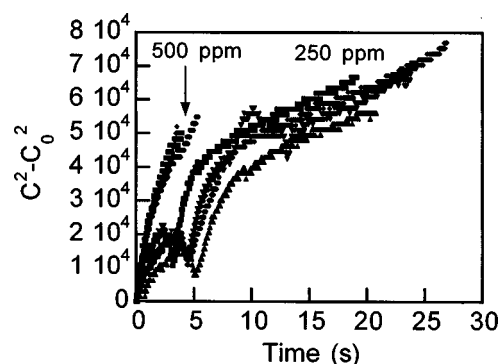


FIG. 8. Effect of Neodol 91-6 concentration on the drainage of dodecane films. The water phases contain 250 or 500 ppm Neodol 91-6 (4  $\mu$ L drops, 20% compression).

the Marangoni effect.<sup>17</sup> Increasing the surfactant concentration in the bulk phases allows surfactant diffusion and adsorption to decrease the interfacial tension gradient, thus accelerating the drainage rate.

Drainage behavior varies profoundly with the surfactant type. For example, the drainage curves for a system containing an anionic surfactant, SDS (Fig. 9) differ completely from those shown above for systems containing nonionic Neodol 91-6. When the aqueous phases contained 2500 ppm SDS in deionized water, the measured count values first increased, then decreased significantly before rising again to a plateau. This unusual behavior, unlike anything seen in systems containing nonionic surfactant, probably arises due to the charge on the surfactant. Electrostatic interactions certainly control the amount of SDS adsorbed and interfacial rheology. Furthermore, the adsorption of the anionic SDS enhances the formation of electrostatic double layers that contribute to the measured impedance. Thus the equivalent circuit for this system is probably not a simple plane-parallel capacitor.

Upon addition of 1250 ppm NaCl to the aqueous phases, the drainage behavior of the dodecane films changed completely. The added electrolyte screened the electrostatic interaction so that the SDS behaved more like a nonionic surfactant. The drainage curves therefore resemble, at least qualitatively, those shown earlier for Neodol 91-6.

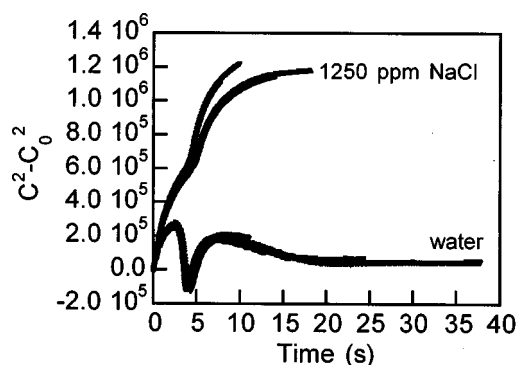


FIG. 9. Effect of added salt on the drainage of dodecane films in contact with water phases containing 2500 ppm SDS in pure water or 1250 ppm aqueous NaCl solution (4  $\mu$ L drops, 20% compression).

### C. Discussion

The results presented here provide a few examples from a large body of experimental observations. In general, the features of oil film drainage curves obtained using the TFIA are remarkably sensitive to the amount, type, and location of surfactants in the oil and water phases. Drainage curves are also sensitive to the values of user-specified parameters, including drop volume, equilibration time, and percentage compression. These observations suggest that the TFIA may have considerable utility as a screening tool for selecting appropriate surfactants for emulsion formulations. Current research aims to correlate thin film drainage behavior obtained from the TFIA with long-term measurements of emulsion stability. If successful, this work will demonstrate the utility of the TFIA as a tool for accelerated testing of emulsion stability.

At this stage, detailed interpretation of the drainage curves is problematic. Variations in user-specified parameters alter the drainage behavior in seemingly predictable ways. At this time, however, we cannot provide reliable interpretations of count versus time data in terms of film drainage mechanisms and their dependence on surfactant type, concentration, or location. This level of analysis requires a more sophisticated model than the one presented here.

Nevertheless, the results shown above exemplify the rich information content of TFIA drainage curves and motivate the development of a more realistic model. The components of this model include a more realistic equivalent circuit representation of the material in the coalescence cell, drop shape calculations for estimating the applied compressive force and contact area, and a more realistic description of hydrodynamics and mass transfer in thin film draining. This model will

enable us to convert TFIA count values into true film thicknesses. Using a suitable hydrodynamic model of film drainage, we may be able to extract interfacial rheological parameters from thickness versus time data. The TFIA thus represents the first step in the development of a new method with potential utility for characterizing interfacial rheology.

### ACKNOWLEDGMENTS

H.J.P. acknowledges the financial support of this work by the Dow Chemical Company and the U.S. National Science Foundation through Grant No. CTS-9258137. This article is the subject of U.S. Patent 5,542,289 assigned to the Dow Chemical Company.

- <sup>1</sup>A. K. Malhotra and D. T. Wasan, *Thin Liquid Films: Fundamentals and Applications*, edited by I. B. Ivanov (Marcel Dekker, New York, 1988).
- <sup>2</sup>I. B. Ivanov and D. S. Dimitrov, in *Thin Liquid Films*, edited by I. B. Ivanov (Marcel Dekker, New York, 1988).
- <sup>3</sup>A. Scheludko, *Adv. Colloid Interface Sci.* **1**, 391 (1967).
- <sup>4</sup>P. A. Kralchevsky, K. D. Danov, and I. B. Ivanov, in *Foams*, edited by R. K. Prud'homme and S. A. Khan (Marcel Dekker, New York, 1996).
- <sup>5</sup>T. K. Chuang and R. W. Flumerfelt, *Rev. Sci. Instrum.* **68**, 3839 (1997).
- <sup>6</sup>G. Singh, C. A. Miller, and G. J. Hirasaki, *J. Colloid Interface Sci.* **187**, 334 (1997).
- <sup>7</sup>A. D. Nikolov and D. T. Wasan, *Colloids Surf., A* **123/124**, 375 (1997).
- <sup>8</sup>K. P. Velikov, O. D. Velev, K. G. Marinova, and G. N. Constantinides, *J. Chem. Soc., Faraday Trans.* **93**, 2069 (1997).
- <sup>9</sup>T. D. Hodgson and J. C. Lee, *J. Colloid Interface Sci.* **30**, 94 (1969).
- <sup>10</sup>G. E. Scheele and D. E. Leng, *Chem. Eng. Sci.* **26**, 1867 (1971).
- <sup>11</sup>R. W. Flumerfelt, J. P. Oppenheim, and J. R. Son, *AIChE Symp. Ser.* **212**, 113 (1982).
- <sup>12</sup>K. O. Hool and R. C. Saunders, U. S. Patent 5,542,289 (1996).
- <sup>13</sup>K. O. Hool and B. Schuchardt, *Meas. Sci. Technol.* **3**, 451 (1992).
- <sup>14</sup>S. Hartland, *J. Colloid Interface Sci.* **26**, 383 (1968).
- <sup>15</sup>O. Reynolds, *Philos. Trans. R. Soc. London, Ser. A* **177**, 157 (1886).
- <sup>16</sup>T. K. Chuang and R. W. Flumerfelt, *Rev. Sci. Instrum.* **68**, 3839 (1997).
- <sup>17</sup>A. K. Malhotra and D. T. Wasan, *Chem. Eng. Commun.* **55**, 95 (1987).